Water Resources Research

RESEARCH ARTICLE
10.1029/2023WR035092

Key Points:

- Water vapor isotopes provide a reliable proxy for evapotranspiration (*ET*) minus precipitation (*P*) in the Congo Basin
- *ET* contributes over 70% to *P* within the four quadrants of the Congo Basin
- River discharge is highest in the western part of the basin, where there are more rivers and higher flow

Correspondence to:
S. Worden,
sarahrw27@g.ucla.edu

Citation:
Worden, S., Bloom, A. A., Worden, J., Levine, P., Shi, M., & Fu, R. (2024). Congo Basin water balance and terrestrial fluxes inferred from satellite observations of the isotopic composition of water vapor. *Water Resources Research*, *60*, e2023WR035092. https://doi.org/10.1029/2023WR035092

Received 12 APR 2023
Accepted 14 JUN 2024

Author Contributions:
Conceptualization: Sarah Worden, A. Anthony Bloom, John Worden, Paul Levine, Mingjie Shi, Rong Fu
Data curation: Sarah Worden
Formal analysis: Sarah Worden, A. Anthony Bloom, John Worden, Paul Levine, Mingjie Shi, Rong Fu
Funding acquisition: Rong Fu
Writing – original draft: Sarah Worden
Writing – review & editing: Sarah Worden, A. Anthony Bloom, John Worden, Paul Levine, Mingjie Shi, Rong Fu

Congo Basin Water Balance and Terrestrial Fluxes Inferred From Satellite Observations of the Isotopic Composition of Water Vapor

Sarah Worden[1], A. Anthony Bloom[2], John Worden[2], Paul Levine[2], Mingjie Shi[3], and Rong Fu[1]

[1]University of California, Los Angeles, Los Angeles, CA, USA, [2]Jet Propulsion Laboratory, California Institute of Technology, Pasadena, CA, USA, [3]Pacific Northwest National Laboratory, Richland, WA, USA

Abstract Large spatio-temporal gradients in the Congo basin vegetation and rainfall are observed. However, its water-balance (evapotranspiration minus precipitation, or $ET - P$) is typically measured at basin-scales, limited primarily by river-discharge data, spatial resolution of terrestrial water storage measurements, and poorly constrained *ET*. We use observations of the isotopic composition of water vapor to quantify the spatio-temporal variability of net surface water fluxes across the Congo Basin between 2003 and 2018. These data are calibrated at basin scale using satellite gravity and total Congo river discharge measurements and then used to estimate time-varying $ET - P$ over four quadrants representing the Congo Basin, providing first estimates of this kind for the region. We find that the multi-year record, seasonality, and interannual variability of $ET - P$ from both the isotopes and the gravity/river discharge based estimates are consistent. Additionally, we use precipitation and gravity-based estimates with our water vapor isotope-based $ET - P$ to calculate time and space averaged *ET* and net river discharge within the Congo Basin. These quadrant-scale moisture flux estimates indicate (a) substantial recycling of moisture in the Congo Basin (temporally and spatially averaged $ET/P > 70\%$), consistent with models and visible light-based *ET* estimates, and (b) net river outflow is largest in the Western Congo where there are more rivers and higher flow rates. Our results confirm the importance of *ET* in modulating the Congo water cycle relative to other water sources.

Plain Language Summary Rainfall and vegetation vary substantially across the Congo Basin. However, the spatial variations, seasonality, and interannual variability of the net water balance, (the difference between evapotranspiration and rainfall) is not well quantified. Atmospheric observations of the isotopic composition of water vapor are sensitive to the balance of evapotranspiration (*ET*) and precipitation (*P*). We calibrate new observations of the isotopic composition of water vapor to $ET - P$ that is based on satellite gravity measurements and ground-based river discharge measurements to quantify $ET - P$ across four quadrants of the Congo basin. When combined with satellite measurements of rainfall, we show that ET is the largest source of Congo basin water vapor. As *ET* is about 70% of observed rainfall, vegetation therefore plays an outsized role on the Congo water cycle. Additionally, when combined with satellite measurements of gravity, we show that river discharge is higher in the western part of the basin, where there are more rivers and stronger flows.

1. Introduction

The Congo Basin, home to the world's second largest tropical rainforest and river by discharge volume, as well as the largest peatland complex in the tropics, is a crucial region for the Earth's water and carbon cycles (e.g., Alsdorf et al., 2016; Dargie et al., 2017). The basin accounts for approximately 30% of Africa's total rainfall and nearly half of its freshwater discharge to the Atlantic Ocean (e.g., Brummett et al., 2009; Laraque et al., 2013; N'kaya et al., 2022). Previous studies have documented decadal changes in rainfall, changes in its rainy season onsets and length, and declines in terrestrial water storage within the basin since the beginning of the 21st century (e.g., Jiang et al., 2019; Nicholson et al., 2022; Zhou et al., 2014). As carbon and water cycles in the tropics are tightly coupled (e.g., Gentine et al., 2019; Green et al., 2017), these changes to the water cycle can have significant effects on vegetation in the Congo Basin (e.g., Fung et al., 2005; Saeed et al., 2013; Zhou et al., 2014). The difference between evapotranspiration minus precipitation ($ET - P$), provides a measure of the net water flux leaving the soil to the atmosphere (e.g., Feng & Zhang, 2015; Fung et al., 2005; Shi et al., 2022). Consequently, $ET - P$ estimates are directly sensitive to the coupling between the atmosphere and terrestrial vegetation (e.g., Davis et al., 2019; Dong et al., 2020; Guan et al., 2015; Hakamada et al., 2020) with positive values ($ET - P > 0$)

10.1029/2023WR035092

indicating soil moisture deficits and subsequent plant stress (e.g., Aragão et al., 2007; Guan et al., 2015; Tao et al., 2022; Zemp et al., 2017).

However, data set uncertainties and sampling remain a challenge for accurately closing the Congo terrestrial water balance and its corresponding fluxes (e.g., Azarderakhsh et al., 2011; Moreira et al., 2019; Sheffield et al., 2009), especially as the water balance represents the difference between two large fluxes:

$$ET - P = -\frac{Q}{A} - \frac{dS}{dt} \quad (1)$$

where ET is evapotranspiration, P is precipitation, Q is the volumetric river discharge, A is the area of the basin studied, S is the water storage anomaly within the basin expressed as an equivalent water height, and t is time.

Satellite-based estimates of P and ET in the Congo Basin are subject to large uncertainties due to cloud cover and rainfall interference (e.g., Chambers et al., 2007; Shi et al., 2022; Wan, 2008), leading to large disparities between data sets (e.g., Nicholson et al., 2018; Weerasinghe et al., 2020). As a result, many studies have turned to the water balance as an alternative, combining river discharge and changes in terrestrial water storage to estimate $ET - P$ (e.g., Azarderakhsh et al., 2011; Burnett et al., 2020; Moreira et al., 2019; Rodell, Famiglietti, et al., 2004, Rodell, Houser, et al., 2004; Rodell et al., 2011; Sheffield et al., 2009; Shi et al., 2022). While changes in terrestrial water storage recently available via GRACE gravity estimates (Wahr et al., 2004) are mainly precision-limited and provide information on below-ground water fluxes, they have relatively coarse resolution compared to other P and ET estimates (e.g., Landerer & Swenson, 2012; Reager et al., 2016; Wahr et al., 2004). Additionally, the uncertainty of in-situ river discharge measurements across the Congo Basin, is unknown (e.g., Alsdorf et al., 2016; Burnett et al., 2020). Consequently, water balance estimates using these surface-based measurements typically are of the entire Congo Basin (Burnett et al., 2020).

However, we should expect that water balance in the Congo Basin exhibits significant spatial and temporal variation because P varies substantially across the basin at seasonal to decadal time scales (e.g., Nicholson, 2022). The northern hemisphere region experiences bi-annual rainy seasons with a very weak summer dry season in June, July, and August, while the southern hemisphere region experiences a single rainy season in the boreal fall (September-October-November) and winter (December-January-February) (Figure 1). The southern hemisphere receives less rainfall during the dry season and more rainfall during the peak of the rainy season, resulting a greater seasonal variation than that of the northern hemisphere. P seasonality and interannual variations also differ between the western and eastern basin (e.g., Balas et al., 2007; Mba et al., 2022), particularly as mesoscale convective systems that provide much of the rainfall for the basin increase in frequency toward the equator and the interior of the continent (Jackson et al., 2009).

River flows within the seven identified sub-basin drainage systems also exhibit significant spatial and temporal variation (e.g., N'kaya et al., 2022). The Northwest quadrant ($Quad_{NW}$) contains parts of the Lower Congo, Middle Congo, Oubangui, and Sangha and Ruki sub-basins, and fully contains the Sanga River. The Northeast quadrant ($Quad_{NE}$) contains parts of the Oubangui, Middle Congo, Ruki, Upper Congo, and a small part of the Tanganyika sub-basins. The Southwest quadrant ($Quad_{SW}$) contains parts of the Kasai, Ruki, Lower Congo, and "Below Kinshasa-Brazzaville" Congo sub-basins, and fully contains the Kasai river. The Southeast quadrant ($Quad_{SE}$) contains parts of the Kasai, Lomami, Upper Congo, and Tanganyika sub-basins (Alsdorf et al., 2016; N'kaya et al., 2022). However, contemporary discharge data only exists for three out of the six drainage systems. The Cuvette Centrale in the northwestern basin, which hosts the tropic's largest peatland complex in the world (Dargie et al., 2017), lacks in situ measurements in general. Many studies rely on indirect approaches such as remote sensing and modeling to estimate river discharge for many of these drainage systems (e.g., Alsdorf et al., 2016; N'kaya et al., 2022; Tshimanga & Hughes, 2014). Therefore, observation-based data limitations have prevented the systematic evaluation of these spatial and temporal differences in the water budget and their relationship with biomass within the Congo Basin.

In this manuscript, we employ a newly developed approach (Bailey et al., 2017; Shi et al., 2022; J. Worden et al., 2019) for quantifying $ET - P$ using satellite observations of the isotopic composition of water vapor. We improve upon prior estimates of $ET - P$ averaged over the entire Congo Basin using gravity and river discharge data (e.g., Burnett et al., 2020). Those estimates are limited to the entire basin, whereas the satellite isotope measurements can resolve spatial gradients in the atmospheric water balance (Shi et al., 2022). We show using the

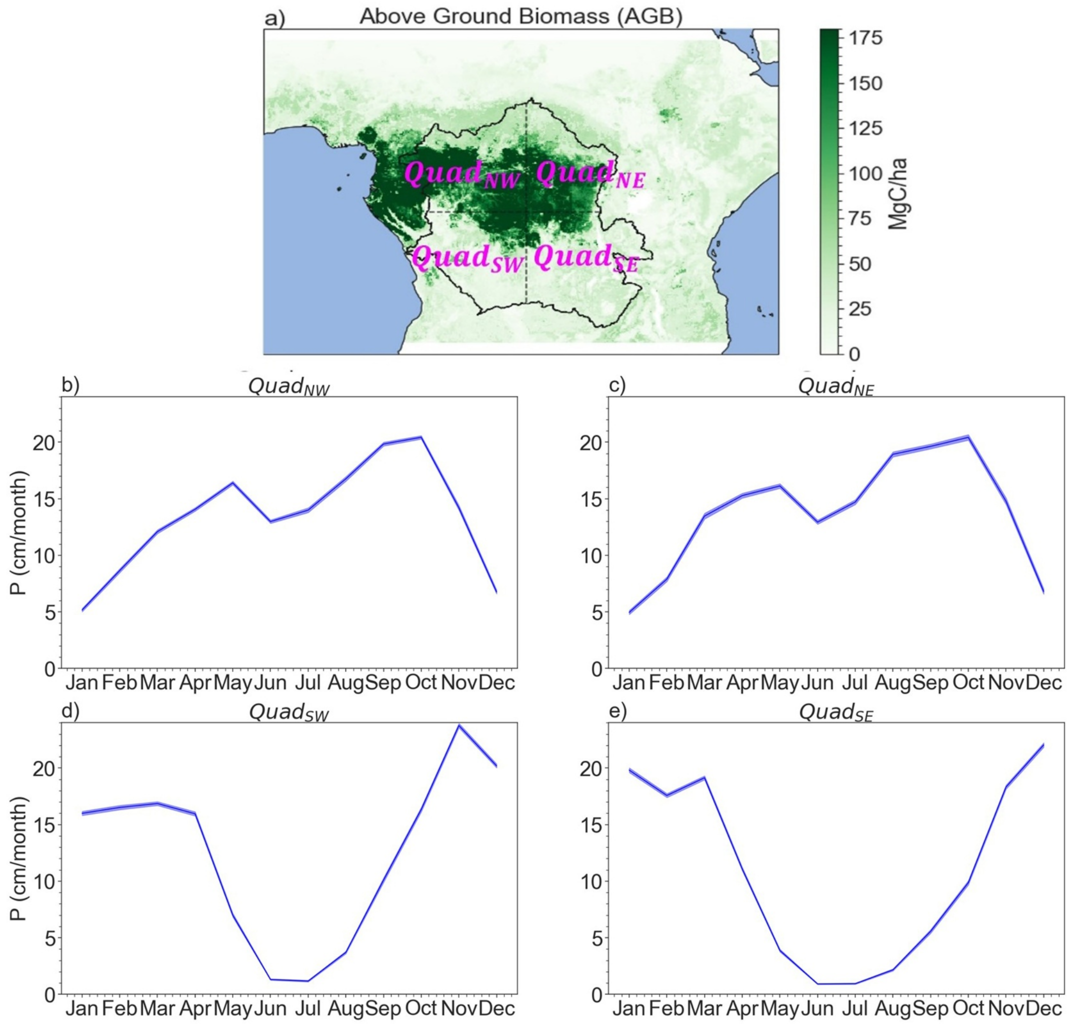

Figure 1. (a) Satellite-based observations of above-ground biomass (AGB) averaged over 2000–2019. The black outline represents the area of the Congo Basin, and the dashed lines divide the basin into four subbasin quadrants: $Quad_{NW}$, $Quad_{NE}$, $Quad_{SW}$, and $Quad_{SE}$; (b)–(e) Seasonal precipitation averaged over 2003–2018 for the four quadrants. The different quadrants are separated by a vertical dashed line at 23°E and a horizontal dashed line at 2°S. Error is the standard error of the mean.

isotopically-enabled version of the Community Atmospheric Model Version 5 (iCAM) climate model (Section 2.3) that these data can resolve $ET - P$ in four quadrants of the Congo basin (we describe this as "quadrant scale"). In addition, both the gravity-based terrestrial water storage and isotope data are essentially precision limited (Aumann et al., 2019; Rodell, Famiglietti, et al., 2004: Rodell, Houser, et al., 2004) for the spatial scales considered here, allowing for improved confidence in the monthly to interannual to decadal variation of atmospheric water balance in these regions. We use these water balance estimates to calculate new time and space-averaged, quadrant-scale ET and net river discharge estimates additionally using measurements of quadrant-scale P and terrestrial water storage (TWS) changes. We can then use these estimates to examine space and time variability in key moisture fluxes within the basin as well as compare our ET estimates to other ET estimates that are calculated using modeling and/or reanalysis. While we cannot deduce whether our estimated $ET - P$, ET, and net river discharge are more accurate than existing products because of a lack of validation data, we can compare those products to our estimates to check for consistency.

10.1029/2023WR035092

2. Data and Methods

In this section, we first discuss the sources of data for our study (2.1). We then demonstrate how we can use satellite observations of water vapor isotopes (or deuterium content of water vapor) to quantify $ET - P$ using simulations from iCAM (Sections 2.2-2.3).

2.1. Data Sources

We list our data sources for *ET*, *P*, changes in terrestrial water storage, river discharge, and aboveground biomass (AGB). We use multiple different sources for *ET* and *P* to compare to our calculated $ET - P$ and *ET* products as well as explore the spread in *ET* and *P* products over the Congo Basin. The data sources for the water vapor isotopes are described in Section 2.2. The data sources for model verification of our methodology are described in Section 2.3.

ET: We use the following *ET* data sets in our study:

1. We use the Global Land Evaporation Amsterdam Model (GLEAM) v3.6b total *ET*, which is based on satellite data and the Priestly Taylor model (e.g., Martens et al., 2017; Miralles et al., 2011) to separately estimate the different components of *ET*.
2. We use the Global Land Data Assimilation System (GLDAS) L4 v2.1 GLDAS_NOAH025_M *ET* product available between 2000 and 2022 at monthly time steps (Beaudoing and Rodell, 2019; Rodell, Famiglietti, et al., 2004; Rodell, Houser, et al., 2004).
3. We use the Priestly Taylor- Jet Propulsion Laboratory (PT-JPL) *ET* data that is created by combining reanalysis and the Moderate Resolution Imaging Spectroradiometer (MODIS) observations (Fisher et al., 2008).
4. We use the MODIS MOD16A3GF_006_ET_500m total yearly *ET* product, which is based on the Penman-Monteith equation (Running et al., 2021).
5. We use the Fifth Generation of the European Center for Medium-Range Weather Forecasts (ECMWF) Reanalysis (ERA5) monthly mean of daily means of the surface latent heat flux, which is then converted to *ET*. The reanalysis combines observations with model forecasts to estimate dynamic and thermodynamic atmospheric quantities (Hersbach et al., 2020).

P: We use the following *P* data sets in our study:

1. We use the Tropical Rainfall Measuring Mission (TRMM) 3B43 gridded, monthly *P* estimates that are generated using a combination of microwave and radar sensors calibrated with gauge data from the Global Precipitation Climatology Center (GPCC) (Huffman et al., 2007). We use TRMM *P* estimates to evaluate $ET - P$ and *ET* in this study as this data set performs well in this region (Nicholson et al., 2018); a comparison of other *P* products to TRMM *P* is found in the Supplementary.
2. We use the Climate Hazards Group InfraRed Precipitation with Station data (CHIRPS), Version 2.0 monthly *P* available from 1981 to near-present (Funk et al., 2015).
3. We use the Precipitation Estimation from Remotely Sensed Information using Artificial Neural Networks-Climate Data Record (PERSIANN-CDR), monthly *P* produced using the PERSIANN algorithm on infrared satellite data and trained on National Centers for Environmental Prediction (NCEP) *P* data (Ashouri et al., 2015).

Gravity-Based Water Storage Anomalies: In addition, basin-scale water storage anomalies (*S*) come from the GRACE satellite (Landerer & Swenson, 2012) calculated by Burnett et al. (2020) using the arithmetic mean of the GRACE solutions on 1° grids from GeoForschungsZentrum Potsdam (GFZ), Jet Propulsion Laboratory (JPL), and Center for Space Research at the University of Texas at Austin (CSR) (e.g., Burnett et al., 2020; Sakumura et al., 2014; Wahr et al., 2006). Quadrant-scale water storage anomalies come from the same centers, GFZ, JPL, and CSR, and are the GRACE/GRACE-FO Mascon Ocean, Ice, and Hydrology Equivalent Water Height RL06 V2 at 0.5° spatial resolution available between 2002 and 2021 (Landerer et al., 2020; Loomis et al., 2019; Save, 2020; Save et al., 2016; Watkins et al., 2015; Wiese et al., 2019).

Water storage anomalies (*S*) from GRACE are converted to *dS*/*dt* using a centered-difference approach at the monthly timescale (Khorrami et al., 2023; Landerer et al., 2010; Lehmann et al., 2022):

$$\frac{dS}{dt_n} = \frac{(S_{n+1} - S_{n-1})}{2\Delta t} \quad (2)$$

where Δt is 1 month. The uncertainty of the dS/dt is calculated as half the difference between the highest and lowest dS/dt values from the three GRACE S solutions in any given month (Burnett et al., 2020; Lee et al., 2011).

River Discharge: River discharge estimates come from the SO-HYBAM river discharge (Q) measurements from a station located at Kinshasa-Brazzaville. The area of the Congo Basin (A) is found using the HydroSHEDS 15 arcsec boundary for the Congo Basin, which produces a total basin area of 3,705,220 km^2 (Burnett et al., 2020; Lehner et al., 2008). Error in river discharge measurements is poorly characterized within this region (e.g., Alsdorf et al., 2016; Burnett et al., 2020; Kitambo et al., 2022). Prior studies have noted a range of uncertainties between 5% and 20% for these discharge measurements (Burnett et al., 2020; O'Loughlin et al., 2020). We assume a 20% error in the Q/A measurements to be consistent with Burnett et al. (2020) as we use some of their provided estimates in our study; however, this is likely to be conservative especially as the observed gauge is quite inland and can provide a good representation of the upstream discharge (e.g., Alsdorf et al., 2016).

AGB: AGB is estimated by Xu et al. (2021) using a combination of lidar, global modeling, and satellite data. The following steps were taken to produce these estimates: (a) Ground inventory plots (>100,000 in number) are integrated with airborne and satellite data, with models used to relate lidar-derived metrics and radar backscatter to AGB estimates from ground plots; (b) Spatially aggregated samples of woody vegetation AGB mean and variance at 10-km spatial resolution are developed using satellite and airborne lidar as training data; and (c) AGB is estimated by using the training data in spatial-temporal machine learning models. The satellite data used in the process come from the Ice, Cloud, and land Elevation Satellite (ICESAT), the Shuttle Radar Topography Missions (SRTM), the Advanced Land Observing Satellite (ALOS), Landsat, the Moderate Resolution Imaging Spectroradiometer (MODIS), and QuikSCAT (QSCAT). More details on this product can be found in Xu et al. (2021).

2.2. Deuterium Content of Water (δD) and *dd*04

Bailey et al. (2017) and Shi et al. (2022) have demonstrated the use of satellite observations of tropospheric water vapor deuterium content in estimating $ET - P$. This can be achieved by normalizing the deuterium content to a representative water vapor value in the free troposphere. Covariation between the normalized deuterium content and $ET - P$ holds in tropical regions with significant mixing between the surface and atmosphere. The deuterium content of water is expressed as the relative ratio of the number of HDO molecules to the total number of H_2O molecules in parts per thousand (‰) relative to the isotopic composition of ocean water as shown below (Equation 3):

$$\delta D = 1000 \times \left(\frac{R - R_{std}}{R_{std}}\right) \quad (3)$$

where R is the ratio of the number of HDO molecules to the total number of H_2O molecules and R_{std} is the corresponding ratio in a reference standard, taken here to be the Vienna Standard Mean Ocean Water: $R_{std} = 3.11 \times 10^{-4}$ (e.g., Wright et al., 2017 and references therein). A mixture of air parcels originating from different sources influences the isotopic composition of water vapor in the free troposphere (Galewsky, 2018; Galewsky & Hurley, 2010). Through analysis of the isotopic compositions of air parcels, we can trace their sources to either vegetation or ocean because δD values contributed by ocean evaporation are distinctively different from those by rainforest ET. A further discussion on δD estimates can be found in J. Worden et al. (2021).

To calculate δD, we use single pixel tropospheric retrievals of HDO and H_2O between 230 and 912 hPa from the Atmospheric Infrared Sounder (AIRS) radiances using the optimal estimation. We use AIRS data instead of those from the Tropospheric Emission Spectrometer (J. Worden et al., 2007) due to its longer record and greater sampling. The AIRS data is bias corrected as suggested by Herman et al. (2020) due to smoothing and systematic errors, as well as instrument noise. We first normalize the deuterium content of water vapor to a reference water vapor concentration of 4 mmol mol^{-1} by (a) regressing the observed HDO profile against the observed H_2O

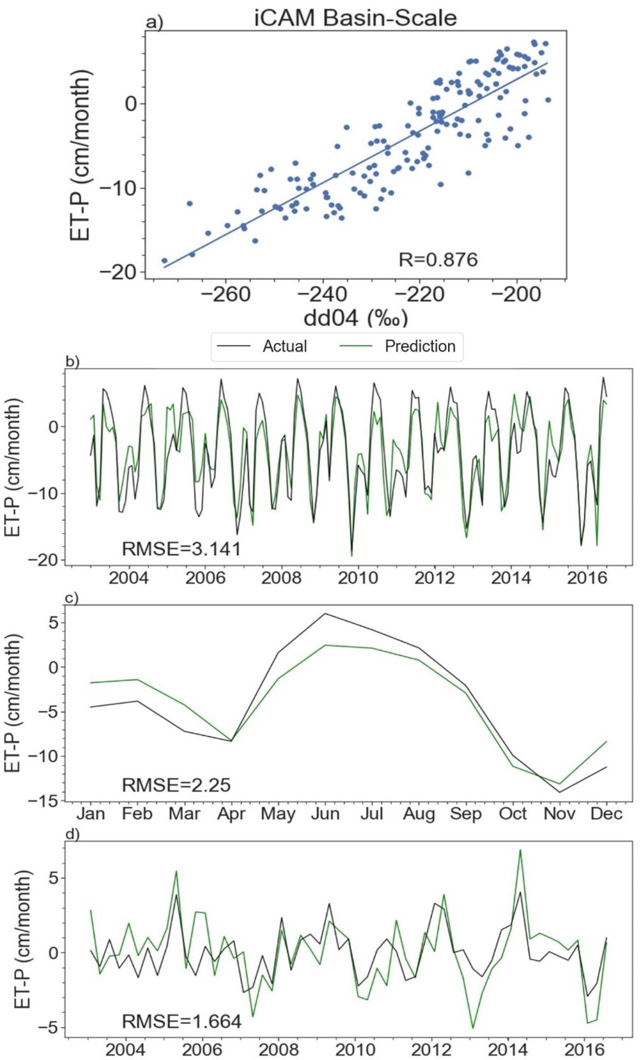

Figure 2. (a) Linear regression of the iCAM *dd*04 estimates (after projecting through the AIRS observation operator) and the iCAM $ET-P$ on a basin scale; (b)–(d): Multi-year, seasonal cycle, and inter-annual variations (IAVs) of model estimates of $ET-P$ compared to regression-based $ET-P$. IAVs have been resampled to a seasonal resolution to better compare; the monthly resolution and associated RMSE are described in the Supplementary.

profile; and (b) calculating the HDO value that matches a reference H_2O of 4 mmol/mol (Bailey et al., 2017). From the resulting HDO and H_2O values, we obtain a proxy for atmospheric water balance that we refer to as *dd*04.

2.3. iCAM Model Relationships Between *dd*04 and $ET-P$ in the Congo Basin

In this section, we demonstrate the linear relationship between *dd*04 and $ET-P$ in the Congo Basin on basin and quadrant-scale using the isotopically enabled version of the Community Atmosphere Model 2 (iCAM; Danabasoglu et al., 2020; Shi et al., 2022). We demonstrate the linear regression between modeled *dd*04 and $ET-P$ on a basin-scale in Figure 2a. To compare to the AIRS *dd*04 data, we calculate an "AIRS view" of the iCAM model *dd*04, as recommended in the TROPESS AIRS HDO/H2O Level 2 User Guide and Validation Document (J. Worden et al., 2019). We thus project the iCAM model HDO and H_2O profiles through the AIRS observation operator provided with the AIRS data. Additionally, we use iCAM and AIRS HDO/H2O data between 230 and 912 hPa, as we find that the iCAM regression performs better using this pressure range compared to the suggested AIRS pressure range for this data in the User Guide, 400–825 mb (not shown). As illustrated in Figure 2, the modeled $ET-P$ and *dd*04 exhibit a well-correlated relationship ($R = 0.876$). Using this basin-scale linear regression, we find $ET-P$ using iCAM measurements via the following equation:

$$ET - P = 0.31 \times dd04 + 64.29 \quad (4)$$

In Figures 2b–2d, we compare the $ET-P$ iCAM record from 2003 to 2017, its seasonality, and interannual variations to those calculated using Equation 4. Note that the RMSE for Figure 2d applies to the IAVs rescaled temporally to the seasonal level to better visually compare the predicted versus actual $ET-P$ IAVs. The RMSE value for the monthly IAV's can be found in the Supplementary. This $ET-P/dd04$ relationship exhibits the strongest performance during dry season months, but the weakest performance during wet season months (Figure 2c). This weaker performance could be due to additional isotopic processes that are more frequent during rainy seasons and can change measured δD (e.g., Galewsky et al., 2016) and masks the original isotopic signal. For example, heavier water vapor isotopes preferentially condense, thus depleting δD during rainfall events. Furthermore, large-scale convergence of air masses during deep convection can bring in relatively depleted water vapor that overtakes any enrichment from surface *ET*. More descriptions of how these processes can affect the isotopic composition of water vapor, or possible confounding factors of this relationship can be found in Galewsky et al. (2016) and Bailey et al. (2017).

As discussed previously, basin-scale river discharge estimates limit water balance estimates based on gravity and river discharge data to the entire basin. Similar to the approach taken by Shi et al. (2022) in the Amazon, the new deuterium-based estimates of $ET-P$ offer an opportunity to improve on the spatial knowledge of $ET-P$, ET, and $\frac{Q}{A}$ estimates in the Congo. We first calibrate the basin-scale, deuterium-based $ET-P$ with the terrestrial water storage and river discharge data. Then, using these same regression coefficients, with *dd*04 averaged over the four quadrants (Figure 1a), we estimate $ET-P$ in the four quadrants. We use these same regression coefficients, instead of re-calculating these coefficients for each quadrant, because the river discharge measurements are only available on a basin scale. We choose to limit this calculation to four quadrants as the basin-scale linear regression coefficients do not perform well at estimating $ET-P$ on smaller than quadrant scale (not shown).

To evaluate the uncertainty of this method, we calculate the RMSE between modeled and actual $ET-P$ within the basin using iCAM data, following the methodology outlined in Shi et al. (2022), as lack of data in this region

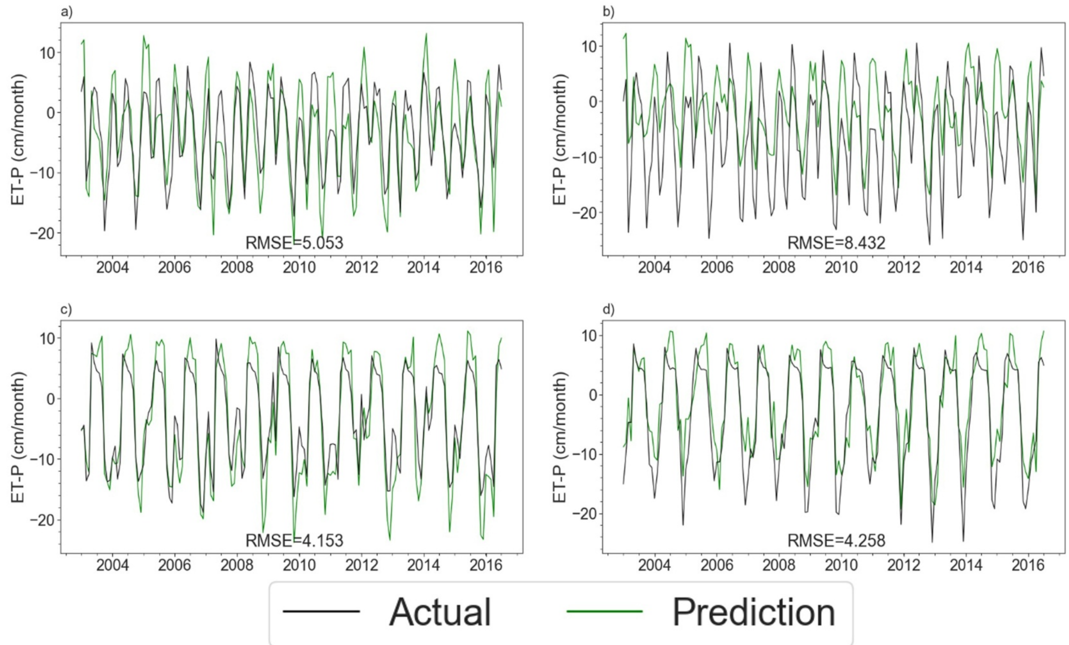

Figure 3. Multi-year record of iCAM $ET - P$ (black) and regression-estimated $ET - P$ (green) using the basin-scale regression equation for each quadrant: (a) $Quad_{NW}$; (b) $Quad_{NE}$; (c) $Quad_{SW}$; and (d) $Quad_{SE}$.

prevents us from evaluating this uncertainty empirically. Figures 3–5 show the difference between $ET - P$ over each quadrant using iCAM, as well as the calculated RMSE between the predicted $ET - P$ and modeled $ET - P$ for the long-term record, seasonal, and interannual variations, respectively. To improve visual ease of comparison, we scale the interannual variability to seasonal values; the monthly IAVs are shown in the Supplementary.

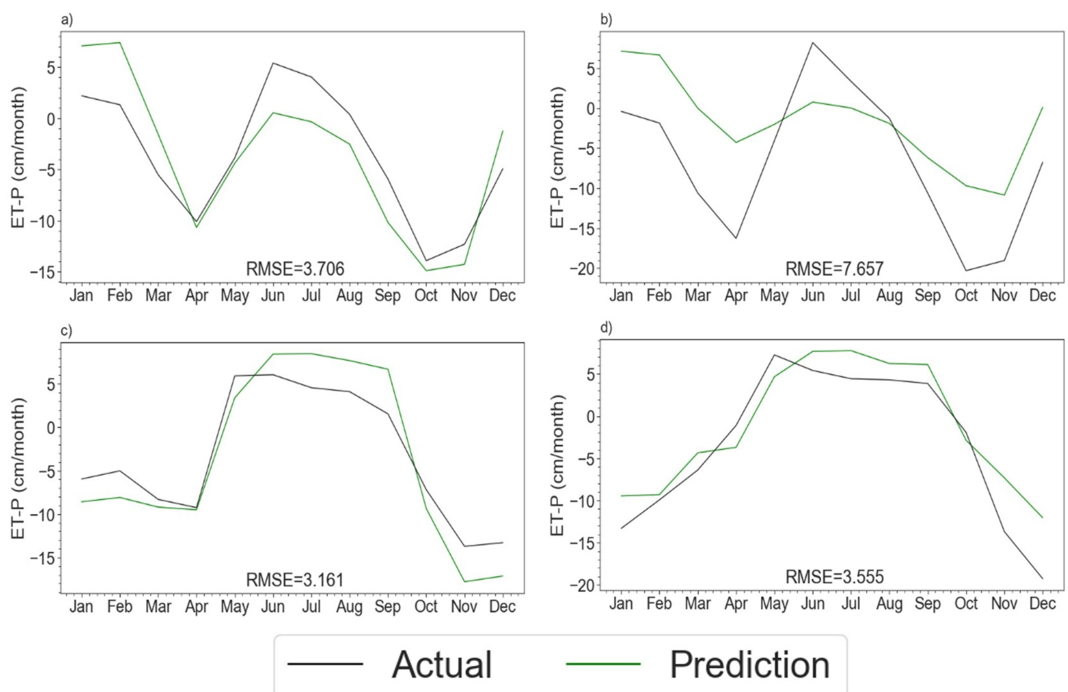

Figure 4. Seasonality of iCAM $ET - P$ (black) and regression-estimated $ET - P$ (green) using the basin scale regression equation for each quadrant: (a) $Quad_{NW}$; (b) $Quad_{NE}$; (c) $Quad_{SW}$; and (d) $Quad_{SE}$.

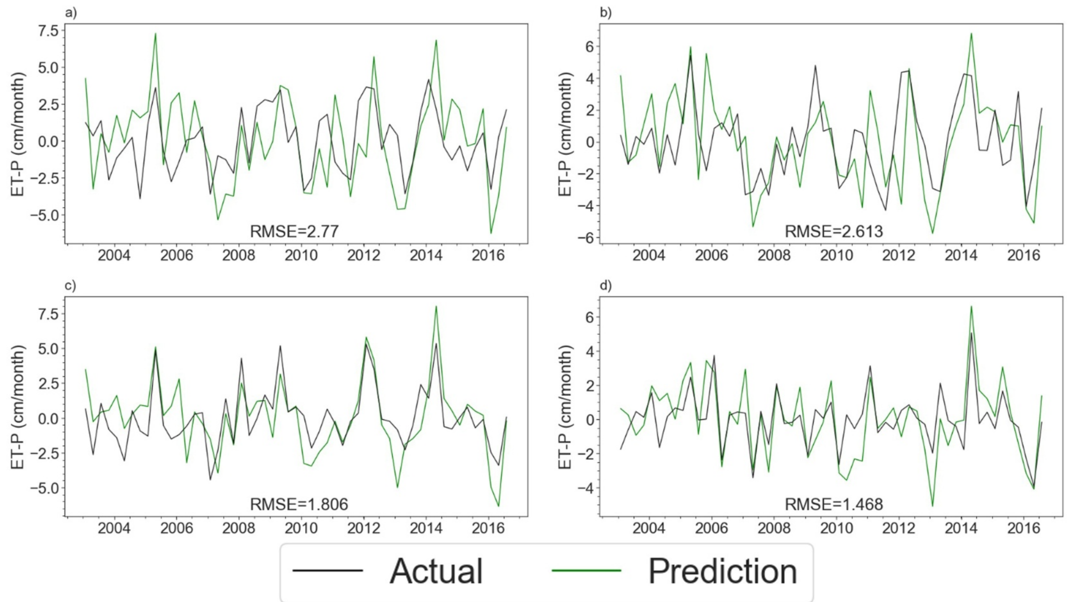

Figure 5. Interannual variations (IAVs) of iCAM $ET - P$ (black) and regression-estimated $ET - P$ (green) using the basin-scale regression equation for each quadrant: (a) $Quad_{NW}$; (b) $Quad_{NE}$; (c) $Quad_{SW}$; and (d) $Quad_{SE}$.

The regressions perform best in capturing the interannual variability and show better overall performance in the southern hemisphere than in the northern hemisphere. The regression is less effective in $Quad_{NE}$, which has the highest RMSE errors (Figures 3–5). It is possible that these higher errors are introduced because mesoscale convective systems are more prominent within this region (e.g., Jackson et al., 2009), which could introduce large scale changes in δD from convective processes such as rainfall re-evaporation without large scale changes in atmospheric humidity (Bailey et al., 2017). Additionally, model error could add to these uncertainties.

3. Results

3.1. Observationally-Based, Basin-Scale Relationships Between $dd04$ and $ET - P$

We can expect that a linear relationship between $dd04$ measurements and $ET - P$ exists because the sensitivity of water vapor isotopes to large-scale water cycle processes can be used to distinguish evaporation versus precipitation dominated environments. These environments determine large scale moisture flux diverge or convergence, such that when normalizing the isotope ratio to a fixed specific humidity, water vapor isotopes should be able to distinguish between these two regimes (Bailey et al., 2017). Previous studies thus show that this relationship exists most strongly within the tropics, but also persists globally (Shi et al., 2022; Singh et al., 2023).

However, because there is a considerable range of ET and P products in the Congo Basin, as discussed in several studies (da Motta Paca et al., 2019; Negrón Juárez et al., 2009; Nicholson & Klotter, 2021; Pan et al., 2020; Sun et al., 2018; Weerasinghe et al., 2020, Supplementary), using ET and P directly from these data to estimate water balance is less reliable. Instead, we utilize the surface water balance (right hand side of Equation 1) to quantify a linear relationship. Basin-scale $\frac{dS}{dt}$ and $\frac{Q}{A}$ data are taken from a public data set generated by Burnett et al. (2020); their sources are described in the previous section.

Using these basin-scale measurements, we calculate $ET - P$ using the following equation:

$$ET - P = 0.12 \times dd04 + 12.12 \tag{5}$$

Figure 6 illustrates the linear relationship between $-\frac{Q}{A} - \frac{dS}{dt}$ and $dd04$ derived from AIRS, along with the multi-year record, seasonality, and IAVs of our calculated $ET - P$. A comparison between our results and other remotely-sensed and reanalysis ET and P products is available in the Supplementary. We calculate both the accuracy and precision errors of our estimated $ET - P$ using the AIRS $dd04$ estimates. We assume that the

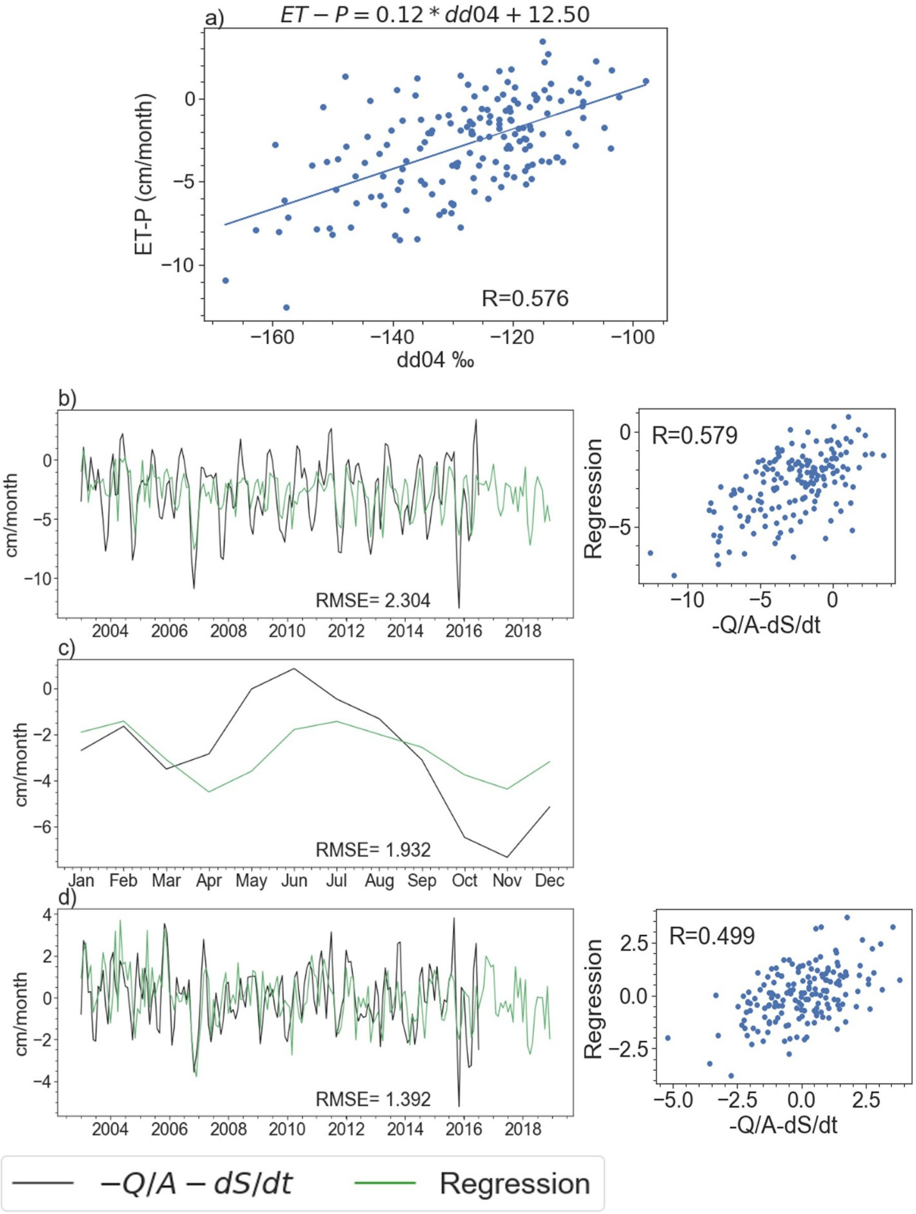

Figure 6. (a) Basin-scale linear regression between AIRS $dd04$ measurements and $-\frac{Q}{A} - \frac{dS}{dt}$; (b) long-term record of our calculated $ET - P$ compared to $-\frac{Q}{A} - \frac{dS}{dt}$ as well as a scatter plot showing the linear relationship between them; (c) seasonality of our calculated $ET - P$ compared to $-\frac{Q}{A} - \frac{dS}{dt}$; and (d) interannual variations of our calculated $ET - P$ compared to $-\frac{Q}{A} - \frac{dS}{dt}$ as well as a scatter plot showing the linear relationship between them.

accuracy errors in the GRACE terrestrial water storage estimates, as well as the errors in the AIRS $dd04$ estimates are small compared to the river discharge error, which is unknown and has been assigned an estimated error of 20% (Burnett et al., 2020; Landerer & Swenson, 2012; Shi et al., 2022). Therefore, we assume that the error in the Q/A estimates dominates the error in $-\frac{Q}{A} - \frac{dS}{dt}$. However, this error in $-\frac{Q}{A} - \frac{dS}{dt}$ will change based on the season. As there are certain times within the year when $\frac{dS}{dt} = 0$, we choose a final accuracy error of $0.2 \times \frac{Q}{A}$ to apply to our $ET - P$ estimates. Therefore, we report a time-averaged accuracy error of 0.56 cm/month. For the precision error, we calculate the error using first principles:

Table 1
ET and ET/P Averaged Over Time and the Entire Congo Basin for Different ET Data Sets

	Mean *ET* (cm/month)	Mean *ET/P*
Regression-Based	9.71 ± 0.94	0.77 ± 0.02
ET_{wb} (Burnett et al., 2020)	9.75 ± 0.94	0.76 ± 0.02
MODIS	10.25 ± 0.04	0.83 ± 0.01
Fisher et al. (2008)	8.34 ± 1.3	0.67 ± 0.02
GLEAM	9.47 ± 1.93	0.77 ± 0.02
GLDAS	9.60 ± 0.04	0.77 ± 0.01
ERA5	11.12 ± 0.04	0.90 ± 0.01

Note. Precipitation comes from TRMM.

$$(ET-P)_{err} = \sqrt{Q_{err}^2 + \frac{dS^2}{dt}_{err}} \tag{6}$$

The precision error for basin-scale $ET - P$ is 0.91 cm/month.

Our calculated $ET - P$ (Figure 6b) compares well with $-\frac{Q}{A} - \frac{dS}{dt}$ (hereafter referred to as discharge/gravity water balance) although it does not generally capture extreme discharge/gravity water balance values. We examine both the seasonality and IAVs to determine the cause. Our calculated seasonal $ET - P$ (Figure 6c) remains below zero throughout the year, whereas the seasonal discharge/gravity water balance goes above zero during May-June. While the overall seasonal change agrees are consistent between the deuterium and gravity based measurements, the deuterium based $ET - P$ does not capture the same extreme highs and lows as the discharge/gravity water balance estimates. On the other hand, the interannual variability of the deuterium-based water balance is consistent with the discharge/gravity water balance, generally matching the sign of the anomalies and how they change over time: both over short-time scales (within a year) and over long-term time scales, that is, over the whole record. For example, both data sets show higher values in the earlier part of the record, lower values near 2007, and similar variations near zero thereafter. Furthermore, discharge/gravity water balance IAVs indicate large atmospheric water balance variability between 2015 and 2017, during which an extreme El Niño event (Santoso et al., 2017) induced severe drought within the basin via increases in both soil moisture and atmospheric water stress (Rifai et al., 2019). Our calculated $ET - P$ IAVs match the direction but not the magnitude of the anomalies.

3.2. Estimates of *ET* and *ET/P* for the Entire Congo Basin

We next estimate basin-scale *ET* estimates using our regression-based water balance estimates. Simply adding *P* to our calculated $ET - P$ yields an unrealistic *ET* seasonality, as we find that *P* dominates the atmospheric water balance variability (Supplementary). Only when we additionally average in time does our calculated *ET* compare well with other existing *ET* estimates. We compare our calculated *ET* to the following data sets: MODIS *ET*, water-balance calculated *ET* from Burnett et al. (2020), GLDAS ET, PT-JPL *ET* from Fisher et al. (2008), and GLEAM *ET* (Table 1).

We calculate the errors for the following *ET* data sets using the time-averaged standard error of the mean: MODIS, GLEAM, ERA5, PT-JPL (Fisher et al., 2008), and GLDAS ET products. The error in ET_{WB} and regression-based *ET* is calculated using first principles, with the regression-based *ET* error in particular calculated by:

$$ET_{err} = \sqrt{\left(\frac{\mathrm{RMSE}_{ET-P}}{\sqrt{n}}^2 + P_{err}^2\right)} \tag{7}$$

where the RMSE is the RMSE between the iCAM $ET - P$ and iCAM regression-based $ET - P$, n is the length of the time series, and P_{err} is the standard error of the mean of the TRMM *P* estimates. We additionally use this to calculate the error on *ET* on quadrant scales.

Our calculated *ET*, 9.71 cm/month, compares well with water-balance *ET*, GLEAM *ET*, and GLDAS *ET* with a range of 9.47–9.75 cm/month. MODIS and ERA5 *ET* are higher, 10.25 cm/month and 11.12 cm/month, respectively. *ET* estimates from Fisher et al. (2008), which combines MODIS and reanalysis *ET* products, has the lowest *ET* estimate at 8.34 cm/month.

We also compare the contribution of *ET* to *P* (*ET*/*P*) using TRMM *P* and *ET* from the previously mentioned data sets. We use the following to calculate the error in $\frac{ET}{P}$:

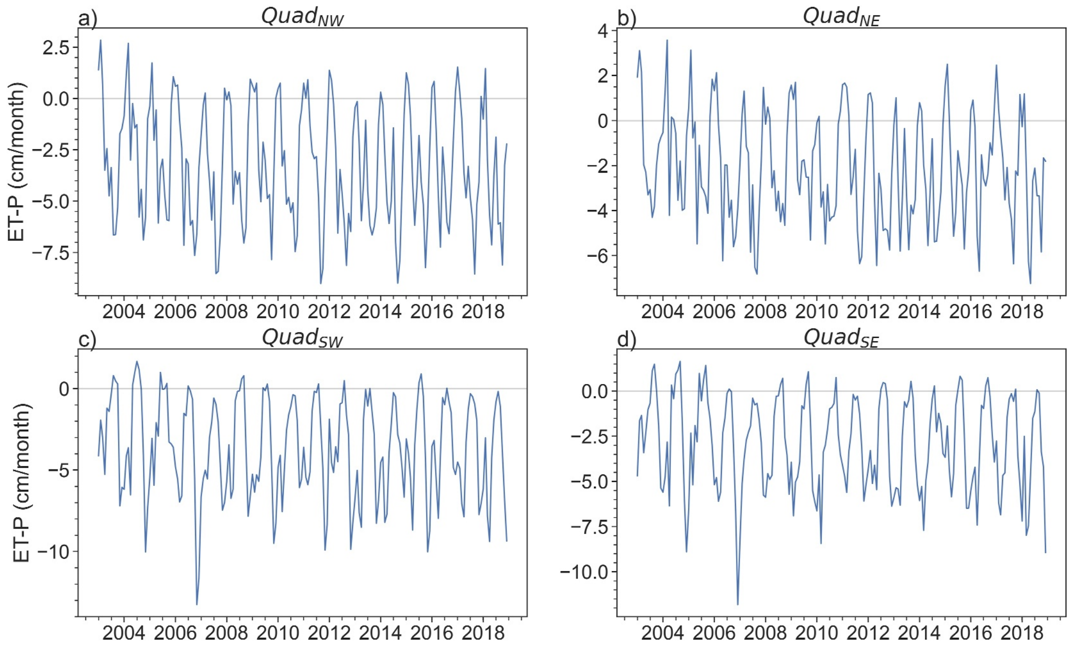

Figure 7. ET − P multi-year record for each quadrant calculated using the basin-scale linear relationship.

$$\left(\frac{ET}{P}\right)_{err} = \sqrt{\frac{ET_{err}}{ET}^2 + \frac{P_{err}}{P}^2} \tag{8}$$

where ET_{err} is the error in the ET products as described above. We use this to additionally calculate the error in ET/P on quadrant scales.

Our analysis reveals a large contribution (67%–90%) of ET toward P, consistent with previous studies (e.g., Sorí et al., 2022, S. Worden et al., 2021; Risi et al., 2013). This suggests that the contribution of atmospheric moisture flux convergence (MFC) to P $\left(\frac{MFC}{P}\right)$, should range between 10% and 33%. While no MFC observations exist over the Congo Basin, ERA5 reanalysis estimates suggest that MFC contributes about 18% contribution of MFC to P on a basin-scale. MODIS ET best closes this moisture flux budget (83% contribution of ET to P), but our calculated ET estimates, GLEAM, and GLDAS also perform well in closing this budget.

3.3. Estimating $ET - P$ in Four Quadrants

We next calculate quadrant-scale $ET - P$ using quadrant-averaged dd04 measurements in the basin-scale linear regression equation (Equation 5). Because we do not have river discharge at these scales, we estimate the accuracy in $ET - P$ by applying the RMSEs shown in the iCAM model (Section 2.3) for our $ET - P$ multi-year record, seasonality, and IAVs (Figures 7–9).

Seasonally, $ET - P$ is greater than zero in January and February in the northern hemisphere, consistent with low P (less than 5 cm/month, Figure 1b). However, P is only slightly greater during December when the seasonal $ET - P$ is less than zero, indicating an increase in ET during January and February as the Congo transitions to its spring rainy season. In the southern hemisphere, seasonal P drops to near-zero during JJA (Figure 1b); seasonal $ET - P$ also near or above zero (Figures 8c and 8d) indicates that ET decreases significantly during the JJA dry season as well. This is consistent with observed decreases in solar-induced fluorescence (SIF), a proxy for photosynthesis and hence ET (Frankenberg et al., 2011), over the Southern Congo during this period (Jiang et al., 2023).

3.4. Estimating ET, ET/P, and Q/A in Each Quadrant

We next calculate quadrant-scale ET, ET/P, and Q/A using the deuterium-based $ET - P$ estimates. We compare our estimates to other ET products. Such estimates are useful for examining quadrant-scale variabilities in the

10.1029/2023WR035092

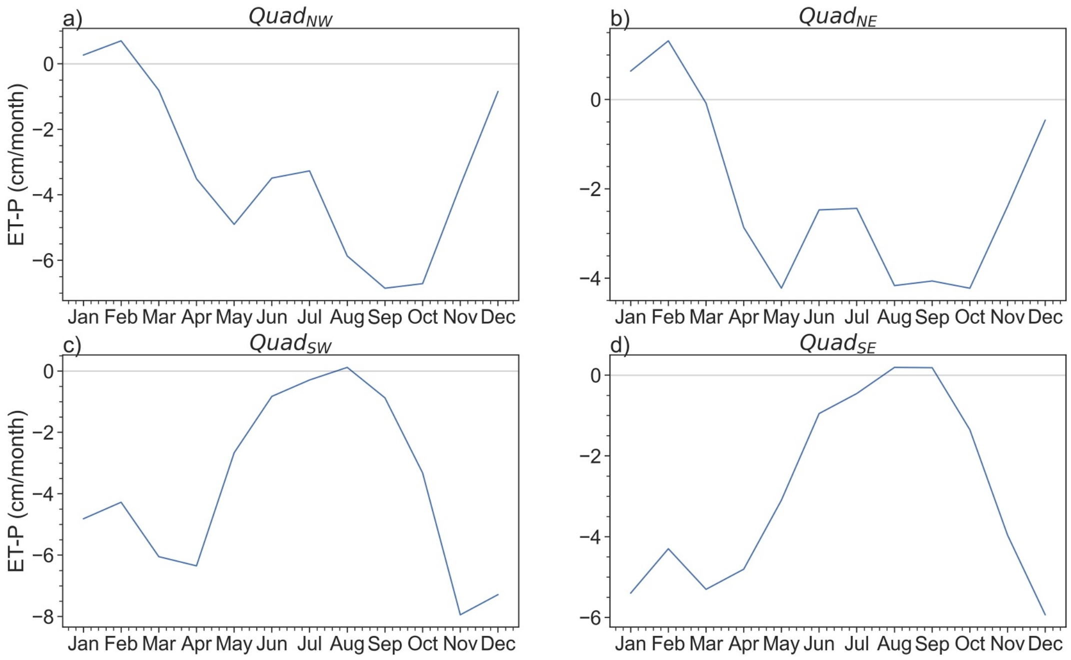

Figure 8. ET − P seasonal cycle for each quadrant calculated using the basin-scale linear relationship.

Congo Basin moisture fluxes that could indicate different moisture regimes, and hence different responses to climatic changes such as the observed decline in April-June rainfall (Nicholson et al., 2022). We calculate *ET* by adding *P* to $ET - P$ for each quadrant. Similarly, we calculate net river discharge (Q/A) by adding GRACE dS/dt estimates to $ET - P$ for each quadrant. All calculations are averaged over both space and time.

We calculate the error in Q/A by:

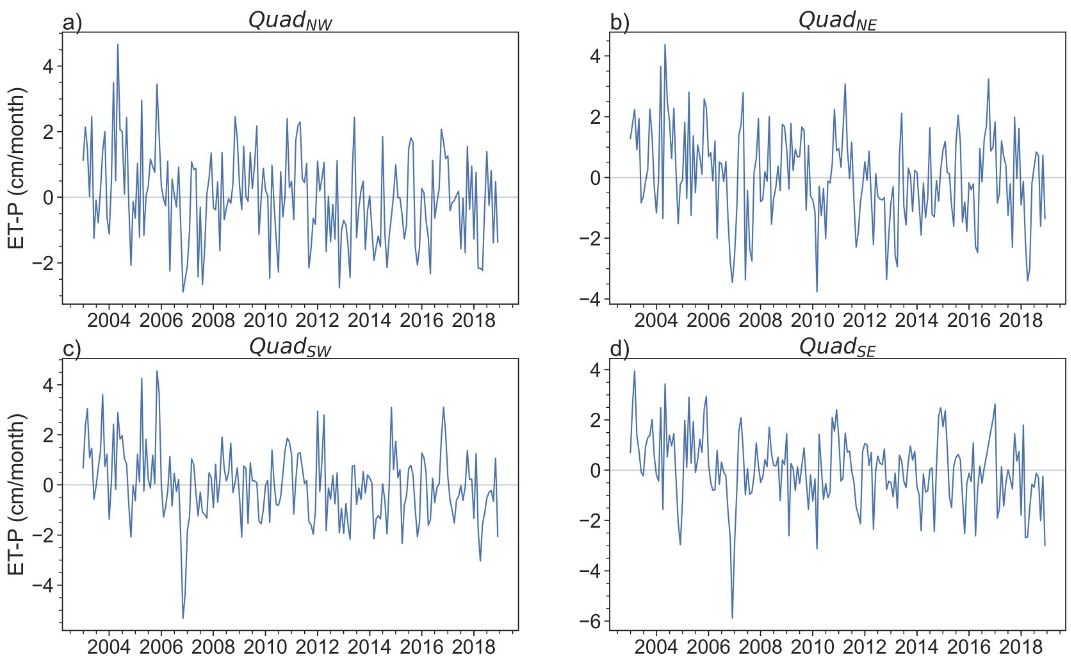

Figure 9. ET − P IAV's for each quadrant calculated using the basin-scale linear relationship.

Table 2
ET, ET/P, and Q/A Averaged Over Time and Space for Each Quadrant

	$Quad_{NW}$			$Quad_{NE}$			$Quad_{SW}$			$Quad_{SE}$		
	ET	*ET/P*	*Q/A*	*ET*	*ET/P*	*Q/A*	*ET*	*ET/P*	*Q/A*	*ET*	*ET/P*	*Q/A*
Regression-based	10.20 ± 0.56	0.76 ± 0.06	2.93 ± 1.32	11.73 ± 0.67	0.84 ± 0.07	1.87 ± 1.35	8.70 ± 0.45	0.70 ± 0.06	3.57 ± 1.28	8.83 ± 0.43	0.73 ± 0.06	2.81 ± 1.36
MODIS	10.88 ± 0.05	0.81 ± 0.01	2.37 ± 1.30	10.43 ± 0.04	0.75 ± 0.01	3.29 ± 1.25	9.26 ± 0.04	0.74 ± 0.01	3.00 ± 1.27	10.41 ± 0.1	0.95 ± 0.01	0.65 ± 1.35
PT-JPL	9.00 ± 0.16	0.67 ± 0.02	4.18 ± 1.31	9.13 ± 0.20	0.66 ± 0.02	4.54 ± 1.27	7.90 ± 0.16	0.64 ± 0.02	4.34 ± 1.28	7.44 ± 0.17	0.68 ± 0.02	3.59 ± 1.36
GLEAM	10.38 ± 0.27	0.77 ± 0.04	2.76 ± 1.30	10.72 ± 0.29	0.77 ± 0.04	3.00 ± 1.26	9.18 ± 0.23	0.73 ± 0.04	3.15 ± 1.27	8.32 ± 0.25	0.76 ± 0.04	2.77 ± 1.35
GLDAS	10.93 ± 0.05	0.81 ± 0.01	2.40 ± 1.30	11.31 ± 0.07	0.82 ± 0.01	2.50 ± 1.26	8.61 ± 0.05	0.69 ± 0.01	3.71 ± 1.27	8.09 ± 0.06	0.74 ± 0.01	2.96 ± 1.35
ERA5	12.14 ± 0.05	0.90 ± 0.01	1.04 ± 1.30	12.05 ± 0.05	0.87 ± 0.01	1.62 ± 1.26	10.63 ± 0.05	0.86 ± 0.01	1.57 ± 1.27	10.11 ± 0.06	0.92 ± 0.01	0.91 ± 1.35

Note. Precipitation comes from TRMM. "Regression-based" indicates measurements calculated using the regression-based $ET - P$ estimates. PT-JPL indicates measurements calculated using *ET* from Fisher et al. (2008).

$$\sqrt{ET^2_{err} + P^2_{err} + \frac{dS}{dt}^{2}_{err}} \tag{9}$$

For the *Q/A* calculated using the remotely sensed and reanalysis *ET* products, and the error in *Q/A* using the regression-based $ET - P$ products as:

$$\sqrt{\left(\frac{\mathrm{RMSE}_{ET-P}}{\sqrt{n}}\right)^2 + \frac{dS^2}{dt}_{err}} \tag{10}$$

We first compare our time and space-averaged *ET* estimates to *ET* from MODIS, GLEAM, ERA5, PT-JPL from Fisher et al. (2008), and GLDAS. Unlike the basin scale *ET* estimates which show agreement across data sets, substantial disparity among the *ET* estimates exists between quadrants. We show that *ET* in $Quad_{NW}$ ranges from 9.00 to 12.14 cm/month, *ET* in $Quad_{NE}$ ranges from 9.13 to 12.05 cm/month, *ET* in $Quad_{SW}$ ranges from 7.90 to 10.63 cm/month, and *ET* in $Quad_{SE}$ ranges from 7.44 to 10.41 cm/month. Our regression-based *ET* estimates compare best with GLEAM and GLDAS *ET* estimates for all four quarters. These three *ET* estimates show higher *ET* in $Quad_{NW}$ and $Quad_{NE}$, and lower *ET* in $Quad_{SW}$ and $Quad_{SE}$. These variations generally correspond to biomass variability between the northern and southern hemisphere. For example, the fraction of biomass with values >100 mgC/ha (high biomass overlaps with tropical rainforest parts of the basin, e.g., Verhegghen et al., 2012) are 0.36, 0.24, 0.10, and 0.08 in $Quad_{NW}$, $Quad_{NE}$, $Quad_{SW}$, and $Quad_{SE}$, respectively. Lowest *ET* corresponds with the lowest fraction of high-biomass vegetation in $Quad_{SE}$. However, while $Quad_{NW}$ contains the most high-biomass vegetation, including a large wetland and peatland complex (Alsdorf et al., 2016; Dargie et al., 2017), $Quad_{NE}$ has the highest *ET* except for MODIS *ET*. It is possible that higher *ET* in $Quad_{NE}$ could be due to *ET* transported from other parts of the basin via low-level winds under 850 hPa (S. Worden et al., 2021).

We additionally calculate *ET/P* and *MFC/P* for all four quadrants to understand variations in moisture contributions to *P* in each quadrant. We show that *ET/P* in $Quad_{NW}$ ranges from 0.67 to 0.90, *ET/P* in $Quad_{NE}$ ranges from 0.66 to 0.87, *ET/P* in $Quad_{SW}$ ranges from 0.64 to 0.86, and *ET/P* in $Quad_{SE}$ ranges from 0.68 to 0.95. Our calculated *ET/P* estimates most closely match *ET/P* estimates using GLEAM and GLDAS. These three data sets all show a similar contribution of *ET* to *P* over all four quadrants, with *ET* contributing slightly less to *P* in $Quad_{SW}$ and $Quad_{SE}$. Meanwhile, mean *MFC/P* is 0.12 in $Quad_{NW}$, 0.18 in $Quad_{NE}$, 0.18 in $Quad_{SW}$, and 0.23 in $Quad_{SE}$. This suggests that despite different *P* and vegetation regimes between the northern and southern quadrants, *ET* still significantly contributes to *P* everywhere within the Congo Basin.

We next calculate quadrant-scale, mean net river discharge estimates by adding quadrant-scale $\frac{dS}{dt}$ estimates to our quadrant-scale $ET - P$ estimates. The spatial limitations in GRACE gravity measurements provide additional motivation to limit our calculations to a quadrant-scale (e.g., Shi et al., 2022). The average of our quadrant-scale net river discharge estimates calculated from our regression-based $ET - P$ is equal to the basin-scale mean net river discharge, adding confidence to our results. Similar to basin-scale river discharge estimates, mean net river discharge in all four quadrants is lower than mean *ET*. Additionally, it has a larger range of magnitude between products than our estimates of *ET* as they highly depend on the *ET* and *P* estimates (from TRMM), the two largest-magnitude moisture fluxes in the Congo Basin (Burnett et al., 2020). *ET* estimates closer to the magnitude of *P* estimates result in lower mean *Q/A*, such as *Q/A* estimated from ERA5 or MODIS *ET* (Table 2). The *Q/A* estimates that come from our regression-based $ET - P$, indicate that the western parts of the basin ha the highest mean river discharge. Higher net river discharge in the western part of the basin could be due to the higher number of rivers in that area and higher estimated daily flow (Alsdorf et al., 2016; Munzimi et al., 2019). For example, out of the 60 identified rivers from Alsdorf et al. (2016), 21 rivers lie within $Quad_{NW}$, 13 within $Quad_{NE}$, 11 within $Quad_{SW}$, 13 within $Quad_{SE}$, and 2 rivers are shared between the different quadrants. Furthermore, the part of the Congo River in $Quad_{SW}$ that outlets to the Atlantic Ocean has the highest modeled daily flow rate (Munzimi et al., 2019).

4. Discussion and Conclusions

A range of factors, including climate change, land use and land cover change, and more, affect the atmospheric water balance, $ET - P$. These changes can directly impact *ET* and/or *P*, or affect river discharge and terrestrial water storage (e.g., Suryatmojo et al., 2013). We confirm that mean *ET* is the second highest moisture flux across the basin compared to *P* (the highest moisture flux), river discharge, and moisture flux convergence. This indicates that a significant portion of the moisture that enters the basin undergoes high recycling (Risi et al., 2013; Sorí et al., 2017, 2022; S. Worden et al., 2021). Changes in *ET* from climate or anthropogenic activities could therefore substantively alter the Congo water balance. For example, increased land cover and land use changes to accommodate increasing logging demands, clearing for subsistence agriculture, and a rising need for natural resources due to population growth (Bele et al., 2015; Fuller et al., 2019; Kleinschroth et al., 2019; Tyukavina et al., 2018) can significantly alter forest composition. Frequent and large-scale fires in Africa (e.g., Andela & van der Werf, 2014; Andela et al., 2019), including the Congo Basin, also change forest composition via processes such as directly removing carbon (e.g., Jiang et al., 2023), altering nutrient availability (Bauters et al., 2018, 2021), inducing soil degradation (Juárez-Orozco et al., 2017), and creating edge effects that change local energy, water, and carbon fluxes (Zhao et al., 2021). The anthropogenic fingerprint on the Congo Basin can therefore significantly affect *ET* in the Congo Basin and hence the future of its water cycle.

We anticipate that the Congo Basin water cycle response to climate change and land cover and land use changes may differ from that of the Amazon, where the contribution of *ET* to *P* is lower, ($ET/P \sim 40\%–50\%$; Baker et al., 2021; Swann & Koven, 2017; Xu et al., 2019) and anthropogenic activities differ in their extent (e.g., N'kaya et al., 2022). Furthermore, a lack of observationally-based data prevents us from understanding spatial heterogeneities in this response. This represents a key gap in our understanding of water and carbon cycle changes in the Congo Basin especially considering high spatial differences in its water cycles and vegetation (e.g., Burnett et al., 2020; Nicholson, 2022; N'kaya et al., 2022; Verhegghen et al., 2012), as well as human disturbance (e.g., Adams & Garcia-Carreras, 2023; Jiang et al., 2023). Our study provides new information on quadrant-scale water flux heterogeneity; however, further research is necessary to develop new, observationally-based water flux data sets that allow us to investigate water and carbon cycle heterogeneity on smaller spatial scales.

Data Availability Statement

GLEAM v3.6b *ET* estimates can be downloaded via the GLEAM website: https://www.gleam.eu/. GLDAS L4 2.1 *ET* estimates, TRMM 3b43 *P* estimates, can downloaded using NASA GES DISC: https://disc.gsfc.nasa.gov. Fisher et al. (2008) PT-JPL *ET* estimates can be found at: http://josh.yosh.org/. MODIS MOD16A3GF_006_ET_500m *ET* products can be found at: https://lpdaac.usgs.gov/products/mod16a3gfv006/. ERA5 surface latent heat flux can be found at: https://cds.climate.copernicus.eu/cdsapp#!/home. CHIRPS *P* data can be found at: https://www.chc.ucsb.edu/data/chirps. PERSIANN-CDR *P* data can be found at: https://www.ncei.noaa.gov/products/climate-data-records/precipitation-persiann. Basin-scale changes in terrestrial water-storage estimates and river discharge estimates taken from Burnett et al. (2020) can be found at: https://osf.io/jpvmb/. JPL GRACE Mascon products can be found at: https://podaac.jpl.nasa.gov/grace-fo. GFZ GRACE Mascon products can be found at: https://isdc.gfz-potsdam.de/grace-isdc/. CSR GRACE Mascon products can be found at: https://www2.csr.utexas.edu/grace/RL06_mascons.html. AIRS dd04 measurements can be found at: https://avdc.gsfc.nasa.gov/pub/data/satellite/Aura/TES/.AIRs/. iCAM model estimates, $ET - P$ estimates, and other data produced by this paper can be made available upon request to the lead author, Sarah Worden (sarahrw27@g.ucla.edu).

Acknowledgments

This work was supported by the Future Investigators in NASA Earth and Space Science and Technology (FINESST) Grant 80NSSC20K1654 and the National Science Foundation Climate and Large-scale Dynamics Program, Award Number 1917781. It was also partially supported by the U.S. Department of Energy Office of Science Biological and Environmental Research as part of the Terrestrial Ecosystem Science Program through the Next-Generation Ecosystem Experiments (NGEE) Tropics project. PNNL is operated by Battelle Memorial Institute for the U.S. DOE under contract DE-AC05-76RLO1830. Part of the work was carried out at the Jet Propulsion Laboratory, California Institute of Technology, under a contract with the National Aeronautics and Space Administration (NASA).

References

Adams, C. E., & Garcia-Carreras, L. (2023). Detection of land-use change and rapid recovery of vegetation after deforestation in the Congo Basin. *Earth Interactions*, *27*, 1–25. https://doi.org/10.1175/EI-D-22-0020.1

Alsdorf, D., Beighley, E., Laraque, A., Lee, H., Tshimanga, R., O'Loughlin, F., et al. (2016). Opportunities for hydrologic research in the Congo Basin. *Reviews of Geophysics*, *54*(2), 378–409. https://doi.org/10.1002/2016RG000517

Andela, N., Morton, D. C., Giglio, L., Paugam, R., Chen, Y., Hantson, S., et al. (2019). The Global Fire Atlas of individual fire size, duration, speed and direction. *Earth System Science Data*, *11*(2), 529–552. https://doi.org/10.5194/essd-11-529-2019
Andela, N., & van der Werf, G. R. (2014). Recent trends in African fires driven by cropland expansion and El Niño to La Niña transition. *Nature*, *4*(9), 791–795. https://doi.org/10.1038/nclimate2313
Aragão, L. E. O., Malhi, Y., Roman-Cuesta, R. M., Saatchi, S., Anderson, L. O., & Shimabukuro, Y. E. (2007). Spatial patterns and fire response of recent Amazonian droughts. *Geophysical Research Letters*, *34*(7), L07701. https://doi.org/10.1029/2006GL028946
Ashouri, H., Hsu, K., Sorooshian, S., Braithwaite, D. K., Knapp, K. R., Cecil, L. D., et al. (2015). PERSIANN-CDR: Daily precipitation climate data record from multisatellite observations for hydrological and climate studies. *Bulletin of the American Meteorological Society*, *96*(1), 69–83. https://doi.org/10.1175/BAMS-D-13-00068.1
Aumann, H. H., Broberg, S., Manning, E., & Pagano, T. (2019). Radiometric stability validation of 17 years of AIRS data using sea surface temperatures. *Geophysical Research Letters*, *46*(21), 12504–12510. https://doi.org/10.1029/2019GL085098
Azarderakhsh, M., Rossow, W. B., Papa, F., Norouzi, H., & Khanbilvardi, R. (2011). Diagnosing water variations within the Amazon basin using satellite data. *Journal of Geophysical Research*, *116*(D24), D24107. https://doi.org/10.1029/2011JD015997
Bailey, A., Blossey, P. N., Noone, D., Nusbaumer, J., & Wood, R. (2017). Detecting shifts in tropical moisture imbalances with satellite-derived isotope ratios in water vapor. *Journal of Geophysical Research*, *122*(11), 5763–5779. https://doi.org/10.1002/2016JD026222
Baker, J. C. A., Garcia-Carreras, L., Gloor, M., Marsham, J. H., Buermann, W., da Rocha, H. R., et al. (2021). Evapotranspiration in the Amazon: Spatial patterns, seasonality, and recent trends in observations, reanalysis, and climate models. *Hydrology and Earth System Sciences*, *25*(4), 2279–2300. https://doi.org/10.5194/hess-25-2279-202
Balas, N., Nicholson, S. E., & Klotter, D. (2007). The relationship of rainfall variability in west central Africa to sea-surface temperature fluctuation. *International Journal of Climatology*, *27*(10), 1335–1349. https://doi.org/10.1002/joc.1456
Bauters, M., Drake, T. W., Verbeeck, H., Bodé, S., Hervé-Fernández, P., Zito, P., et al. (2018). High fire-derived nitrogen deposition on central African forests. *Proceedings of the National Academy of Sciences*, *115*(3), 549–554. https://doi.org/10.1073/pnas.1714597115
Bauters, M., Drake, T. W., Wagner, S., Baumgartner, S., Makelele, I. A., Bodé, S., et al. (2021). Fire-derived phosphorus fertilization of African tropical forests. *Nature Communications*, *12*(1), 1–8. https://doi.org/10.1038/s41467-021-25428-3
Beaudoing, H., Rodell, M., & NASA/GSFC/HSL (2019). *GLDAS Noah Land Surface Model L4 monthly 0.25 x 0.25 degree V2.0, Greenbelt, Maryland, USA*. Goddard Earth Sciences Data and Information Services Center (GES DISC). https://doi.org/10.5067/9SQ1B3ZXP2C5
Bele, M. Y., Sonwa, D. J., & Tiani, A. M. (2015). Adapting the Congo Basin forests management to climate change: Linkages among biodiversity, forest loss, and human well-being. *Forest Policy and Economics*, *50*, 1–10. https://doi.org/10.1016/j.forpol.2014.05.010
Brummett, R. E., Tanania, C., Pandi, A., Ladel, J., Munzimi, Y., Russell, A., et al. (2009). Ressources en eau et biens et services liés à l'écosystème forestier. In C. Wasseige, D. Devers, P. de Marcen, R. Eba'a Atyi, R. Nasi, & P. Mayaux (Eds.) *Les forêts du Bassin du Congo*. Office des publications de l'Union européenne. https://doi.org/10.2788/32456
Burnett, M. W., Quetin, G. R., & Konings, A. G. (2020). Data-driven estimates of evapotranspiration and its controls in the Congo Basin. *Hydrology and Earth System Sciences*, *24*(8), 4189–4211. https://doi.org/10.5194/hess-24-4189-2020
Chambers, J. Q., Asner, G., Morton, D., Anderson, L., Saatchi, S., Espírito-Santo, F., et al. (2007). Regional ecosystem structure and function: Ecological insights from remote sensing of tropical forests. *Trends in Ecology & Evolution*, *22*(8), 414–423. https://doi.org/10.1016/j.tree.2007.05.001
da Motta Paca, V., Espinoza-Dávalos, G. E., Hessels, T. M., Moreira, D. M., Comair, G. F., & Bastiaanssen, W. G. M. (2019). The spatial variability of actual evapotranspiration across the Amazon River Basin based on remote sensing products validated with flux towers. *Ecol Process*, *8*(1), 6. https://doi.org/10.1186/s13717-019-0158-8
Danabasoglu, G., Lamarque, J.-F., Bacmeister, J., Bailey, D. A., DuVivier, A. K., Edwards, J., et al. (2020). The Community Earth System Model Version 2 (CESM2). *Journal of Advances in Modeling Earth Systems*, *12*, e2019MS001916. https://doi.org/10.1029/2019MS001916
Dargie, G., Lewis, S., Lawson, I., Ifo, S. A., Mitchard, E. T. A., Page, S., & Bocko, Y. (2017). Age, extent and carbon storage of the central Congo Basin peatland complex. *Nature*, *542*(7639), 86–90. https://doi.org/10.1038/nature21048
Davis, K. T., Dobrowski, S. Z., Holden, Z. A., Higuera, P. E., & Abatzoglou, J. T. (2019). Microclimatic buffering in forests of the future: The role of local water balance. *Ecography*, *42*, 1–11. https://doi.org/10.1111/ecog.03836
Dong, G., Zhao, F. Y., Chen, J. Q., Zhang, Y. Q., Shao, C. L., Jiang, S., et al. (2020). Non-climatic component provoked substantial spatiotemporal changes of carbon and water use efficiency on the Mongolian Plateau. *Environmental Research Letters*, *15*(9), 095009–095025. https://doi.org/10.1088/1748-9326/ab9692
Feng, H., & Zhang, M. (2015). Global land moisture trends: Drier in dry and wetter in wet over land. *Scientific Reports*, *5*(1), 1–6. https://doi.org/10.1038/srep18018
Fisher, J. B., Tu, K. P., & Baldocchi, D. D. (2008). Global estimates of the land-atmosphere water flux based on monthly AVHRR and ISLSCP-II data, validated at 16 FLUXNET sites. *Remote Sensing of Environment*, *112*(3), 901–919. https://doi.org/10.1016/j.rse.2007.06.025
Frankenberg, C., Fisher, J. B., Worden, J., Badgley, G., Saatchi, S. S., Lee, J.-E., et al. (2011). New global observations of the terrestrial carbon cycle from GOSAT: Patterns of plant fluorescence with gross primary productivity. *Geophysical Research Letters*, *38*(17), L17706. https://doi.org/10.1029/2011GL048738
Fuller, T. L., Narins, T. P., Nackoney, J., Bonebrake, T. C., Sesink Clee, P., Morgan, K., et al. (2019). Assessing the impact of China's timber industry on Congo Basin land use change. *Area*, *51*(2), 340–349. https://doi.org/10.1111/AREA.12469
Fung, I. Y., Doney, S. C., Lindsay, K., & John, J. (2005). Evolution of carbon sinks in a changing climate. *Proceedings of the National Academy of Sciences*, *102*(32), 11201–11206. https://doi.org/10.1073/pnas.0504949102
Funk, C., Peterson, P., Landsfeld, M., Pedreros, D., Verdin, J., Shukla, S., et al. (2015). The climate hazards infrared precipitation with stations—A new environmental record for monitoring extremes. *Scientific Data*, *2*(1), 1–21. https://doi.org/10.1038/sdata.2015.66
Galewsky, J. (2018). Using stable isotopes in water vapor to diagnose relationships between lower-tropospheric stability, mixing, and low-cloud cover near the island of Hawaii. *Geophysical Research Letters*, *45*(1), 297–305. https://doi.org/10.1002/2017GL075770
Galewsky, J., & Hurley, J. V. (2010). An advection-condensation model for subtropical water vapor isotopic ratios. *Journal of Geophysical Research*, *115*(D16), D16116. https://doi.org/10.1029/2009JD013651
Galewsky, J., Larsen, H. S., Field, R. D., Worden, J. R., Risi, C., & Schneider, M. (2016). Stable isotopes in atmospheric water vapor and applications to the hydrologic cycle. *Reviews of Geophysics*, *54*(4), 809–865. https://doi.org/10.1002/2015RG000512
Gentine, P., Massmann, A., Lintner, B. R., Hamed Alemohammad, S., Fu, R., Green, J. K., et al. (2019). Land–atmosphere interactions in the tropics–A review. *Hydrology and Earth System Sciences*, *23*(10), 4171–4197. https://doi.org/10.5194/hess-23-4171-2019
Green, J., Konings, A., Alemohammad, S., Berry, J., Entekhabi, D., Kolassa, J., et al. (2017). Regionally strong feedbacks between the atmosphere and terrestrial biosphere. *Nature Geoscience*, *10*(6), 410–414. https://doi.org/10.1038/ngeo2957

Guan, K., Pan, M., Li, H., Wolf, A., Wu, J., Medvigy, D., et al. (2015). Photosynthetic seasonality of global tropical forests constrained by hydroclimate. *Nature Geoscience*, *8*(4), 284–289. https://doi.org/10.1038/ngeo2382

Hakamada, R., Hubbard, R., Stape, J., Lima, W., Moreira, G., & Ferraz, S. (2020). Stocking effects on seasonal tree transpiration and ecosystem water balance in a fast-growing Eucalyptus plantation in Brazil. *Forest Ecology and Management*, *466*, 118149. https://doi.org/10.1016/j.foreco.2020.118149

Herman, R. L., Worden, J., Noone, D., Henze, D., Bowman, K., Cady-Pereira, K., et al. (2020). Comparison of optimal estimation HDO/H_2O retrievals from AIRS with ORACLES measurements. *Atmospheric Measurement Techniques*, *13*(4), 1825–1834. https://doi.org/10.5194/amt-13-1825-2020

Hersbach, H., Bell, B., Berrisford, P., Hirahara, S., Horányi, A., Muñoz-Sabater, J., et al. (2020). The ERA5 global reanalysis. *Quarterly Journal of the Royal Meteorological Society*, *146*(730), 1999–2049. https://doi.org/10.1002/QJ.3803

Huffman, G. J., Bolvin, D. T., Nelkin, E. J., Wolff, D. B., Adler, R. F., Gu, G., et al. (2007). The TRMM multisatellite precipitation analysis (TMPA): Quasi-global, multiyear, combined-sensor precipitation estimates at fine scales. *Journal of Hydrometeorology*, *8*(1), 38–55. https://doi.org/10.1175/JHM560.1

Jackson, B., Nicholson, S., & Klotter, D. (2009). Mesoscale convective systems over western equatorial africa and their relationship to large-scale circulation. *Monthly Weather Review*, *137*(4), 1272–1294. https://doi.org/10.1175/2008MWR2525.1

Jiang, X., Albright, R., Creecy, E., Li, K. F., Liang, M. C., Newman, S., et al. (2023). Congo basin rainforest is a net carbon source during the dry season. *Earth and Space Science*, *10*(2), e2022EA002644. https://doi.org/10.1029/2022EA002644

Jiang, Y., Zhou, L., Tucker, C. J., Raghavendra, A., Hua, W., Liu, Y. Y., & Joiner, J. (2019). Widespread increase of boreal summer dry season length over the Congo rainforest. *Nature Climate Change*, *9*(8), 617–622. https://doi.org/10.1038/s41558-019-0512-y

Juárez-Orozco, S. M., Siebe, C., & Fernández y Fernández, D. (2017). Causes and effects of forest fires in tropical rainforests: A bibliometric approach. *Tropical Conservation Science*, *10*, 1940082917737207. https://doi.org/10.1177/1940082917737207

Khorrami, B., Gorjifard, S., Ali, S., & Feizizadeh, B. (2023). Local-scale monitoring of evapotranspiration based on downscaled GRACE observations and remotely sensed data: An application of terrestrial water balance approach. *Earth Science Informatics*, *16*(2), 1–17. https://doi.org/10.1007/s12145-023-00964-2

Kitambo, B. M., Papa, F., Paris, A., Tshimanga, R. M., Frappart, F., Calmant, S., et al. (2022). A long-term monthly surface water storage dataset for the Congo basin from 1992 to 2015. *Earth System Science Data Discussions*, *15*(7), 1–39. https://doi.org/10.5194/essd-15-2957-2023

Kleinschroth, F., Laporte, N., Laurance, W. F., Goetz, S. J., & Ghazoul, J. (2019). Road expansion and persistence in forests of the Congo Basin. *Nature Sustainability*, *2*(7), 628–634. https://doi.org/10.1038/s41893-019-0310-6

Landerer, F. W., Dickey, J. O., & Güntner, A. (2010). Terrestrial water budget of the Eurasian pan-Arctic from GRACE satellite measurements during 2003–2009. *Journal of Geophysical Research*, *115*(D23), D23115. https://doi.org/10.1029/2010JD014584

Landerer, F. W., Flechtner, F. M., Save, H., Webb, F. H., Bandikova, T., Bertiger, W. I., et al. (2020). Extending the global mass change data record: GRACE follow-on instrument and science data performance. *Geophysical Research Letters*, *47*(12), e2020GL088306. https://doi.org/10.1029/2020GL088306

Landerer, F. W., & Swenson, S. C. (2012). Accuracy of scaled GRACE terrestrial water storage estimates. *Water Resources Research*, *48*(4), W04531. https://doi.org/10.1029/2011WR011453

Laraque, A., Bellanger, M., Adèle, G., Guebanda, S., Gulemvuga, G., Pandi, A., et al. (2013). Recent evolution of Congo, Oubangui and Sangha rivers flows. Académie Royale des Sciences de Belgique. *Geogr. Ecol. Trop.*, *37*(1), 93–100.

Lee, H., Beighley, R. E., Alsdorf, D., Jung, H. C., Shum, C. K., Duan, J., et al. (2011). Characterization of terrestrial water dynamics in the Congo Basin using GRACE and satellite radar altimetry. *Remote Sensing of Environment*, *115*(12), 3530–3538. https://doi.org/10.1016/j.rse.2011.08.015

Lehmann, F., Vishwakarma, B. D., & Bamber, J. (2022). How well are we able to close the water budget at the global scale? *Hydrology and Earth System Sciences*, *26*(1), 35–54. https://doi.org/10.5194/hess-26-35-2022

Lehner, B., Verdin, K., & Jarvis, A. (2008). New global hydrography derived from spaceborne elevation data. *Eos Trans. Am Gesphys. Union*, *89*(10), 93–95. https://doi.org/10.1029/2008EO100001

Loomis, B. D., Luthcke, S. B., & Sabaka, T. J. (2019). Regularization and error characterization of GRACE mascons. *Journal of Geodynamics*, *93*(9), 1381–1398. https://doi.org/10.1007/s00190-019-01252-y

Martens, B., Miralles, D. G., Lievens, H., van der Schalie, R., de Jeu, R. A. M., Fernández-Prieto, D., et al. (2017). GLEAM v3: satellite-based land evaporation and root-zone soil moisture. *Geoscientific Model Development*, *10*(5), 1903–1925. https://doi.org/10.5194/gmd-10-1903-2017

Mba, W. P., Vondou, D. A., & Kamsu-Tamo, P. H. (2022). Central African climate. In R. M. Tshimanga, G. D. M. N'kaya, & D. Alsdorf (Eds.), *Congo basin hydrology, climate, and biogeochemistry*. https://doi.org/10.1002/9781119657002.ch2

Miralles, D. G., De Jeu, R. A. M., Gash, J. H., Holmes, T. R. H., & Dolman, A. J. (2011). Magnitude and variability of land evaporation and its components at the global scale. *Hydrology and Earth System Sciences*, *15*(3), 967–981. https://doi.org/10.5194/hess-15-967-2011

Moreira, A., Ruhoff, A., Roberti, D., Souza, V., Rocha, H., & Paiva, R. (2019). Assessment of terrestrial water balance using remote sensing data in South America. *Journal of Hydrology*, *575*, 131–147. https://doi.org/10.1016/j.jhydrol.2019.05.021

Munzimi, Y., Hansen, M., & Asante, K. (2019). Estimating daily streamflow in the Congo Basin using satellite-derived data and a semi-distributed hydrological model. *Hydrological Sciences Journal*, *64*(12), 1472–1487. https://doi.org/10.1080/02626667.2019.1647342

Negrón Juárez, R. I., Li, W., Fu, R., Fernandes, K., & de Oliveira Cardoso, A. (2009). Comparison of precipitation datasets over the tropical South American and African continents. *Journal of Hydrometeorology*, *10*(1), 289–299. https://doi.org/10.1175/2008JHM1023.1

Nicholson, S. E. (2022). The rainfall and convective regime over equatorial Africa, with emphasis on the Congo Basin. In R. M. Tshimanga, G. D. M. N'kaya, & D. Alsdorf (Eds.), *Congo basin hydrology, climate, and biogeochemistry*. https://doi.org/10.1002/9781119657002.ch3

Nicholson, S. E., Klotter, D., Dezfuli, A. K., & Zhou, L. (2018). New rainfall datasets for the Congo Basin and surrounding regions. *Journal of Hydrometeorology*, *19*(8), 1379–1396. https://doi.org/10.1175/JHM-D18-0015.1

Nicholson, S. E., Klotter, D., Zhou, L., & Hua, W. (2022). Recent rainfall conditions in the Congo Basin. *Environmental Research Letters*, *17*(5), 054052. https://doi.org/10.1088/1748-9326/ac61c4

Nicholson, S. E., & Klotter, D. A. (2021). Assessing the reliability of satellite and reanalysis estimates of rainfall in equatorial Africa. *Remote Sensing*, *13*(18), 3609. https://doi.org/10.3390/rs13183609

N'kaya, G. D. M., Laraque, A., Paturel, J.-E., Guzanga, G. G., Mahé, G., & Tshimanga, R. M. (2022). A new look at hydrology in the Congo basin, based on the study of multi-decadal time series. In R. M. Tshimanga, G. D. M. N'kaya, & D. Alsdorf (Eds.), *Congo basin hydrology, climate, and biogeochemistry*. https://doi.org/10.1002/9781119657002.ch8

O'Loughlin, F. E., Neal, J., Schumann, G. J. P., Beighley, E., & Bates, P. D. (2020). A LISFLOOD-FP hydraulic model of the middle reach of the Congo. *Journal of Hydrology*, *580*, 124203. https://doi.org/10.1016/j.jhydrol.2019.124203

Pan, S., Pan, N., Tian, H., Friedlingstein, P., Sitch, S., Shi, H., et al. (2020). Evaluation of global terrestrial evapotranspiration using state-of-the-art approaches in remote sensing, machine learning and land surface modeling. *Hydrology and Earth System Sciences*, *24*(3), 1485–1509. https://doi.org/10.5194/hess-24-1485-2020

Reager, J. T., Gardner, A. S., Famiglietti, J. S., Wiese, D. N., Eicker, A., & Lo, M. H. (2016). A decade of sea level rise slowed by climate-driven hydrology. *Science*, *12;351*(6274), 699–703. https://doi.org/10.1126/science.aad8386

Rifai, S. W., Li, S., & Malhi, Y. (2019). Coupling of El Niño events and long-term warming leads to pervasive climate extremes in the terrestrial tropics. *Environmental Research Letters*, *14*(10), 105002. https://doi.org/10.1088/1748-9326/ab402f

Risi, C., Noone, D., Frankenberg, C., & Worden, J. (2013). Role of continental recycling in intraseasonal variations of continental moisture as deduced from model simulations and water vapor isotopic measurements. *Water Resources Research*, *49*(7), 4136–4156. https://doi.org/10.1002/wrcr.20312

Rodell, M., Famiglietti, J. S., Chen, J., Seneviratne, S. I., Viterbo, P., Holl, S., & Wilson, C. R. (2004). Basin scale estimates of evapotranspiration using GRACE and other observations. *Geophysical Research Letters*, *31*(20), L20504. https://doi.org/10.1029/2004GL020873

Rodell, M., Houser, P. R., Jambor, U., Gottschalck, J., Mitchell, K., Meng, C., et al. (2004). The global land data assimilation system. *Bulletin America Meteorology Social*, *85*(3), 381–394. https://doi.org/10.1175/BAMS-85-3-381

Rodell, M., McWilliams, E. B., Famiglietti, J. S., Beaudoing, H. K., & Nigro, J. (2011). Estimating evapotranspiration using an observation based terrestrial water budget. *Hydrological Processes*, *25*(26), 4082–4092. https://doi.org/10.1002/hyp.8369

Running, S., Mu, Q., Zhao, M., & Moreno, A. (2021). MODIS/terra net evapotranspiration gap-filled yearly L4 global 500m SIN grid V061 [Dataset]. *NASA EOSDIS Land Processes DAAC*. https://doi.org/10.5067/MODIS/MOD16A3GF.061

Saeed, F., Haensler, A., Weber, T., Hagemann, S., & Jacob, D. (2013). Representation of extreme precipitation events leading to opposite climate change signals over the Congo Basin. *Atmosphere*, *4*(3), 254–271. https://doi.org/10.3390/atmos4030254

Sakumura, C., Bettadpur, S., & Bruinsma, S. (2014). Ensemble prediction and intercomparison analysis of GRACE time-variable gravity field models. *Geophysical Research Letters*, *41*(5), 1389–1397. https://doi.org/10.1002/2013GL058632

Santoso, A., Mcphaden, M. J., & Cai, W. (2017). The defining characteristics of ENSO extremes and the strong 2015/2016 El Niño. *Reviews of Geophysics*, *55*(4), 1079–1129. https://doi.org/10.1002/2017RG000560

Save, H. (2020). CSR GRACE and GRACE-FO RL06 mascon solutions v02. https://doi.org/10.15781/cgq9-nh24

Save, H., Bettadpur, S., & Tapley, B. D. (2016). High resolution CSR GRACE RL05 mascons. *Journal of Geophysical Research: Solid Earth*, *121*(10), 7547–7569. https://doi.org/10.1002/2016JB013007

Sheffield, J., Ferguson, C. R., Troy, T. J., Wood, E. F., & McCabe, M. F. (2009). Closing the terrestrial water budget from satellite remote sensing. *Geophysical Research Letters*, *36*(7), L07403. https://doi.org/10.1029/2009GL037338

Shi, M., Worden, J. R., Bailey, A., Noone, D., Risi, C., Fu, R., et al. (2022). Amazonian terrestrial water balance inferred from satellite-observed water vapor isotopes. *Nature Communications*, *13*(1), 2686. https://doi.org/10.1038/s41467-022-30317-4

Singh, N., Pradhan, R., Singh, R. P., & Gupta, P. K. (2023). The role of continental evapotranspiration on water vapour isotopic variability in the troposphere. *Isotopes in Environmental and Health Studies*, *59*(3), 248–268. https://doi.org/10.1080/10256016.2023.2212834

Sorí, R., Nieto, R., Vicente-Serrano, S. M., Drumond, A., & Gimeno, L. (2017). A Lagrangian perspective of the hydrological cycle in the Congo River basin. *Earth System Dynamics*, *8*(3), 653–675. https://doi.org/10.5194/esd-8-653-2017

Sorí, R., Stojanovic, M., Nieto, R., Liberato, M. L., & Gimeno, L. (2022). Spatiotemporal variability of droughts in the Congo River Basin: The role of atmospheric moisture transport. In R. M. Tshimanga, G. D. M. N'kaya, & D. Alsdorf (Eds.), *Congo Basin hydrology, climate, and biogeochemistry*. https://doi.org/10.1002/9781119657002.ch11

Sun, Q., Miao, C., Duan, Q., Ashouri, H., Sorooshian, S., & Hsu, K.-L. (2018). A review of global precipitation data sets: Data sources, estimation, and intercomparisons. *Reviews of Geophysics*, *56*(1), 79–107. https://doi.org/10.1002/2017RG000574

Suryatmojo, H., Fujimoto, M., Yamakawa, Y., Kosugi, K., & Mizuyama, T. (2013). Water balance changes in the tropical rainforest with intensive forest management system. *International Journal of Sustainable Future for Human Security J-SustaiN*, *1*(2), 56–62. https://doi.org/10.24910/jsustain/1.2/5662

Swann, A., & Koven, C. (2017). A direct estimate of the seasonal cycle of evapotranspiration over the Amazon basin. *Journal of Hydrometeorology*, *18*(8), 2173–2185. https://doi.org/10.1175/JHM-D-17-0004.1

Tao, S., Chave, J., Frison, P.-L., Toan, T. L., Ciais, P., Fang, J., et al. (2022). Increasing and widespread vulnerability of intact tropical rainforests to repeated droughts. *Proceedings of the National Academy of Sciences*, *119*(37), e2116626119. https://doi.org/10.1073/pnas.2116626119

Tshimanga, R. M., & Hughes, D. A. (2014). Basin-scale performance of a semidistributed rainfall-runoff model for hydrological predictions and water resources assessment of large rivers: The Congo River. *Water Resources Research*, *50*(2), 1174–1188. https://doi.org/10.1002/2013WR014310

Tyukavina, A., Hansen, M. C., Potapov, P., Parker, D., Okpa, C., Stehman, S. V., et al. (2018). Congo Basin forest loss dominated by increasing smallholder clearing. *Science Advances*, *4*(11), eaat2993. https://doi.org/10.1126/sciadv.aat2993

Verhegghen, A., Mayaux, P., de Wasseige, C., & Defourny, P. (2012). Mapping Congo Basin vegetation types from 300 m and 1 km multi-sensor time series for carbon stocks and forest areas estimation. *Biogeosciences*, *9*(12), 5061–5079. https://doi.org/10.5194/bg-9-5061-2012

Wahr, J., Swenson, S., & Velicogna, I. (2006). Accuracy of GRACE mass estimates. *Geophysical Research Letters*, *33*(6), L06401. https://doi.org/10.1029/2005GL025305

Wahr, J., Swenson, S., Zlotnicki, V., & Velicogna, I. (2004). Time-variable gravity from GRACE: First results. *Geophysical Research Letters*, *31*(11), L11501. https://doi.org/10.1029/2004GL019779

Wan, Z. (2008). New refinements and validation of the MODIS land-surface temperature/emissivity products. *Remote Sensing of Environment*, *140*(1), 59–74. https://doi.org/10.1016/j.rse.2006.06.026

Watkins, M. M., Wiese, D. N., Yuan, D. N., Boening, C., & Landerer, F. W. (2015). Improved methods for observing Earth's time variable mass distribution with GRACE using spherical cap mascons: Improved gravity observations from GRACE. *Journal of Geophysical Research: Solid Earth*, *120*(4), 2648–2671. https://doi.org/10.1002/2014JB011547

Weerasinghe, I., Bastiaanssen, W., Mul, M., Jia, L., & van Griensven, A. (2020). Can we trust remote sensing evapotranspiration products over Africa? *Hydrology and Earth System Sciences*, *24*(3), 1565–1586. https://doi.org/10.5194/hess-24-1565-2020

Wiese, D. N., Yuan, C., Boening, F. W., Landerer, M., & Watkins, M. (2019). JPL GRACE mascon ocean, ice, and hydrology equivalent water height RL06 CRI filtered Version 02. *Ver. 02. PO.DAAC, CA, USA*. https://doi.org/10.5067/TEMSC-3JC62

Worden, J., Noone, D., Bowman, K., Beer, R., Eldering, A., Fisher, B., et al. (2007). Importance of rain evaporation and continental convection in the tropical water cycle. *Nature*, *445*(7127), 528–532. https://doi.org/10.1038/nature05508

Worden, J., Saatchi, S., Keller, M., Bloom, A., Liu, J., Parazoo, N., et al. (2021). Satellite observations of the tropical terrestrial carbon balance and interactions with the water cycle during the 21st century. *Reviews of Geophysics*, *59*(1), e2020RG000711. https://doi.org/10.1029/2020RG000711

Worden, J. R., Kulawik, S. S., Fu, D., Payne, V. H., Lipton, A. E., Polonsky, I., et al. (2019). Characterization and evaluation of AIRS-based estimates of the deuterium content of water vapor. *Atmospheric Measurement Techniques*, *12*(4), 2331–2339. https://doi.org/10.5194/amt-12-2331-2019

Worden, S., Fu, R., Chakraborty, S., Liu, J., & Worden, J. (2021). Where does moisture come from over the Congo Basin? *Journal of Geophysical Research: Biogeosciences*, *126*(8), e2020JG006024. https://doi.org/10.1029/2020JG006024

Wright, J., Fu, R., Worden, J., Chakraborty, S., Clinton, N., Risi, C., et al. (2017). Rainforest-initiated wet season onset over the southern Amazon. *Proceedings of the National Academy of Sciences*, *114*(32), 8481–8486. https://doi.org/10.1073/pnas.1621516114

Xu, D., Agee, E., Wang, J., & Ivanov, V. Y. (2019). Estimation of evapotranspiration of Amazon rainforest using the maximum entropy production method. *Geophysical Research Letters*, *46*(3), 1402–1412. https://doi.org/10.1029/2018GL080907

Xu, L., Saatchi, S., Yang, Y., Yu, Y., Pongratz, J., Bloom, A., et al. (2021). Changes in global terrestrial live biomass over the 21st century. *Science Advances*, *7*(27), eabe9829. https://doi.org/10.1126/sciadv.abe9829

Zemp, D. C., Schleussner, C.-F., Barbosa, H. M. J., Hirota, M., Montade, V., Sampaio, G., et al. (2017). Self-amplified Amazon forest loss due to vegetation-atmosphere feedbacks. *Nature Communications*, *8*(1), 14681. https://doi.org/10.1038/ncomms14681

Zhao, Z., Li, W., Ciais, P., Santoro, M., Cartus, O., Peng, S., et al. (2021). Fire enhances forest degradation within forest edge zones in Africa. *Nature Geoscience*, *14*(7), 479–483. https://doi.org/10.1038/s41561-021-00763-8

Zhou, L., Tian, Y., Myneni, R. B., Ciais, P., Saatchi, S., Liu, Y. Y., et al. (2014). Widespread decline of Congo rainforest greenness in the past decade. *Nature*, *508*(7498), 86–90. https://doi.org/10.1038/nature13265